Solid State Ionics 14 (1984) 319–327
North-Holland, Amsterdam

THE ELECTRODE RESISTANCE OF ZrO_2–Y_2O_3 (–Bi_2O_3) SOLID ELECTROLYTES WITH Pt ELECTRODES

A.J.A. WINNUBST, A.H.A. SCHARENBORG and A.J. BURGGRAAF
Twente University of Technology, Department of Chemical Engineering, Laboratory for Inorganic Chemistry and Materials Science, P.O. Box 217, 7500 AE Enschede, The Netherlands

Received 10 April 1984
Revised manuscript received 4 September 1984

The electrode resistance (R_{el}) at low over-voltages has been determined for Bi_2O_3 free and Bi_2O_3 doped yttria-stabilized zirconia with sputtered platinum electrodes. The anode and cathode resistances are measured separately and are equal. Bi_2O_3 causes a decrease of the electrode resistance at small overvoltage and with $5 \times 10^{-4} < P_{O_2} \leq 1$ atm. The rate determining step for the electrode reaction under the measuring conditions probably is a charge-transfer process in which oxygen adsorbs dissociatively on the bismuth free and associatively on the bismuth doped samples. The complex impedance behaviour of the electrode reaction can be interpreted in terms of R–C circuits in the P_{O_2} range of 10^{-2}–1 atm.

1. Introduction

Solid electrolytes, which show oxygen ion conductivity at elevated temperatures, are interesting materials for use in. e.g., oxygen pumps and oxygen sensors. The electrode processes at the electrolyte–electrode–gas interface play an important role in the efficiency of oxygen pumping devices and in the response speed when used as an oxygen sensor.

The electrochemical behaviour of the electrode–electrolyte systems depends on many factors such as oxygen partial pressure, temperature, structure of the electrode and the chemical composition of electrolyte and electrode materials. Verkerk et al. [1,2] studied the influence of the solid electrolyte on the electrode process using platinum electrodes. The electrode resistance (R_{el}) of stabilized Bi_2O_3 was found to be considerably lower than that of stabilized ZrO_2, especially at high oxygen partial pressures. In many studies Pt paste electrodes are used. These pastes often contain a small percentage of bismuth for which a negative influence on the electrode behaviour has been reported [3,4]. In this paper effect on the electrode resistance has been studied when Bi is incorporated in stabilized zirconia.

Bauerle [5] already noted that R_{el} strongly depends on electrode material, temperature and current treatment of the system. The mechanism of the oxygen transfer process depends on the temperature region in which the electrode behaviour is examined. A dissociative chemisorption process was reported to be the rate determining step on a sputtered platinum-stabilized zirconia system at temperatures above 970 K [6]. At lower temperatures a charge transfer contribution was observed for the electrode behaviour.

The preparation and morphology of the electrodes are generally badly characterized in literature. The electrode morphology, however, has a strong effect on the electrode behaviour. Especially the preparation of stable electrodes with a low diffusion resistance is important and is difficult to realize. Bauerle [5] prepared very porous electrodes by passing a large current (10^4 A/m^2) through the sample for several minutes at 1073 K. This resulted in rather stable electrodes with high values for the electrode (double layer) capacity.

In this study the electrode behaviour is investigated on pure and Bi_2O_3 doped yttria-stabilized zirconia with sputtered porous Pt electrodes, which have been stabilized by annealing treatments. The measurements are performed with a three elctrode dc system in order

to separate the anodic and cathodic resistance [7]. The electrode–electrolyte systems were also investigated by ac impedance measurements which were analysed by means of a nonlinear least squares fitting program.

2. Theory

The overall electrochemical reaction which takes place at the electrode–electrolyte–gas interface can be described as

$$O_2(g) + 4e' + 2V_O^{\bullet\bullet} \underset{c}{\overset{a}{\rightleftharpoons}} 2O_O^X , \tag{1}$$

where a and c denote the anodic and cathodic reaction respectively. The free and occupied oxygen vacancies are denoted by $V_O^{\bullet\bullet}$ and O_O^X. This overall reaction can be split up in different elementary steps:

(1) The adsorption or desorption of molecular oxygen, which can take place dissociatively or associatively.

(2) Diffusion of adsorbed oxygen to or from the reaction site across the surface of the electrode or electrolyte material.

(3) The charge transfer reaction.

(4) Reaction between oxygen anions and charged point defects followed by diffusion in the electrolyte.

The first elementary step is given by either

$$O_2(g) + 2V_{ads} \rightleftharpoons 2O_{ads}, \text{ dissociative} \tag{2a}$$

or

$$O_2(g) + V_{ads} \rightleftharpoons O_{2\,ads}, \text{ associative.} \tag{2b}$$

V_{ads} is a vacant adsorption site, O_{ads} is an adsorbed oxygen atom. The fraction of oxygen adsorption sites that are occupied is given by θ_{ads}. The mass action relation for the reactions (2a) and (2b) can be written in terms of Langmuir adsorption

$$\theta_{ads}/(1 - \theta_{ads}) = K(P_{O_2})^{1/2} , \tag{3a}$$

$$\theta_{ads}/(1 - \theta_{ads}) = KP_{O_2} . \tag{3b}$$

A diffusion step on the material surface, after dissociation of adsorbed oxygen molecules, can be written as:

$$O_{ads} + V_{rs} \rightleftharpoons O_{rs} + V_{ads}, \tag{4}$$

where V_{rs} and O_{rs} are a vacant and occupied reaction sites respectively. The overall charge transfer reaction is given by:

$$O_{rs} + 2e' + V_O^{\bullet\bullet} \rightleftharpoons O_O^X + V_{rs}. \tag{5}$$

This reaction can again be split up in reaction steps in which the formation of several oxygen species O_2^-, O^-, O^{2-} takes place. The relation between current I and overpotential η for the reactions (4) and (5) is given by a modified Butler–Volmer equation, which incorporates a diffusion step [1,7]

$$I = \exp(\alpha_a V^*) - \exp(-\alpha_c V^*) \times [I_0^{-1} + I_{la}^{-1} \exp(\alpha_a V^*) + I_{lc}^{-1} \exp(-\alpha_c V^*)]^{-1} , \tag{6}$$

$$V^* = \eta F/RT , \tag{7}$$

where α_a and α_c are the anodic and cathodic transfer coefficients, respectively, η is the overpotential applied and I_0 is the equillibrium exchange current for the charge-transfer reaction. The anodic and cathodic mass transport limiting currents are denoted by I_{la} and I_{lc} respectively. At low overpotentials, $|V^*| \ll 1$, ohmic behaviour is obtained. Eq. (6) then becomes:

$$I = (\alpha_a + \alpha_c)V^*/(I_0^{-1} + I_{la}^{-1} + I_{lc}^{-1}) \tag{8}$$

and with eq. (7) we find for the electrode resistance (R_{el}):

$$R_{el} = \eta/I = R_{CT} + R_{la} + R_{lc} \approx (I_0^{-1} + I_{la}^{-1} + I_{lc}^{-1}) . \tag{9}$$

It is clear that for I_{la} and $I_{lc} \gg I_0$ the electrode process and consequently R_{el} is determined by the charge-transfer reaction (5) (i.e. $R_{el} = R_{CT} \sim 1/I_0$). The reaction rate of (5) can be expressed in terms of an exchange current, which can be written as [8,9]:

$$I_{0a} = nek_{ra}(1 - \theta_{r.s}) \exp(\alpha_a FE_e/RT) , \tag{10}$$

$$I_{0c} = nek_{rc}\theta_{r.s} \exp(-\alpha_c FE_e/RT) \tag{11}$$

for the anodic and cathodic reaction respectively, where n is the number of elementary charges transferred during the overall reaction ($n = 4$); k_{ra} and k_{rc} are the anodic and cathodic reaction rate constants respectively. The fraction of oxygen reaction sites, which are occupied is given by $\theta_{r.s}$. This fraction is equal to θ_{ads} when mass transport is not rate determining ($\theta_{r.s}$ =

$\theta_{ads} = \theta$). E_e is the equilibrium potential between electrolyte and electrode which is, according to Nernst: $E_e = E_0 + (RT/nF)\ln(C_{0x}/C_{red})$. The anodic and cathodic transfer coefficients, α_a and α_c, can be written as [9]:

$$\alpha_a = (\gamma_a/\nu) + r - r \times \beta, \tag{12}$$

$$\alpha_c = (\gamma_c/\nu) + r \times \beta, \tag{13}$$

where γ_a and γ_c are the number of elementary charges transferred during the overall reaction before the rate determining step (= RDS) of the anodic and cathodic reaction respectively, r is the number of charges transferred in the RDS, β is a symmetry factor usually taken as 1/2 and ν is the number of times the RDS has to occur to complete a cycle of the overall reaction.

The exchange current, I_0, equals I_{0a} as well as I_{0c} under open circuit stationary conditions ($\eta = 0$); so we can write then:

$$(I_{0c})^{\alpha_a} \times (I_{0a})^{\alpha_c} = I_0^{\alpha_a + \alpha_c},$$

which can be written as:

$$I_0 = (I_{0a})^{\alpha_c/(\alpha_a+\alpha_c)} \times (I_{0c})^{\alpha_a/(\alpha_a+\alpha_c)}. \tag{14}$$

Substitution of eqs. (10) and (11) in eq. (14) gives ($\theta_{r.s} = \theta_{ads} = \theta$):

$$I_0 \approx (1-\theta)^{\alpha_c/(\alpha_a+\alpha_c)} \times (\theta)^{\alpha_a/(\alpha_a+\alpha_c)}. \tag{15}$$

The combination of the Langmuir adsorption [eqs. (3a) or (3b) and eq. (15)] results for dissociative and associative adsorption respectively in:

$$I_0 \approx \theta (P_{O_2})^{-\alpha_c/2(\alpha_a+\alpha_c)} \quad \text{or}$$

$$I_0 \approx (1-\theta)(P_{O_2})^{\alpha_a/2(\alpha_a+\alpha_c)} \text{(dissociative)} \tag{16a}$$

and

$$I_0 \approx \theta (P_{O_2})^{-\alpha_c/(\alpha_a+\alpha_c)} \quad \text{or}$$

$$I_0 \approx (1-\theta)(P_{O_2})^{\alpha_a/(\alpha_a+\alpha_c)} \text{ (associative)}. \tag{16b}$$

At *high* oxygen partial pressures all adsorption sites are occupied ($\theta = 1$), so (16a) becomes:

$$I_0 \approx (P_{O_2})^{-\alpha_c/2(\alpha_a+\alpha_c)}. \tag{17}$$

According to eqs. (9) and (17) with charge transfer as RDS:

$$R_{CT} \approx 1/I_0 \approx (P_{O_2})^{\alpha_c/2(\alpha_a+\alpha_c)}. \tag{18a}$$

For associative adsorption and $\theta = 1$ we get:

$$R_{CT} \approx (P_{O_2})^{\alpha_c/(\alpha_a+\alpha_c)}. \tag{18b}$$

In the case of *low* oxygen partial pressures θ is about zero; the P_{O_2} dependence of R_{CT} becomes for dissociative and associative adsorption respectively ($1 - \theta = 1$):

$$R_{CT} \approx (P_{O_2})^{-\alpha_a/2(\alpha_a+\alpha_c)}, \tag{19a}$$

$$R_{CT} \approx (P_{O_2})^{-\alpha_a/(\alpha_a+\alpha_c)}. \tag{19b}$$

The oxygen partial pressure dependence of the electrode resistance as determined by a charge-transfer reaction can now be calculated by means of eqs. (12), (13), (18) and (19) assuming a certain mechanism and these calculations are compared with experimental results.

3. Experimental

The electrolyte materials used in this study are pure and Bi_2O_3 doped yttria-stabilized zirconia ceramics. Some characteristics of the samples are given in

Table 1
Material characteristics of the investigated electrolytes.

System	Synthesis method	Composition (mol%)			Sintering temperature (K)	Relative density (%)	Grain size (μm)
		ZrO_2	$YO_{1.5}$	$BiO_{1.5}$			
ZY17	alkoxide	83	17	–	1680	99	3
ZY21	citrate	79	21	–	1790	95	8
ZYB1 [a]	alkoxide	83	17		1680	99	3
ZYB2	citrate	78	20.6	1.4	1420	96	3

[a] ZYB1 is a ZY17 sample heat-treated in a Bi_2O_3 atmosphere (1 h, 1170 K).

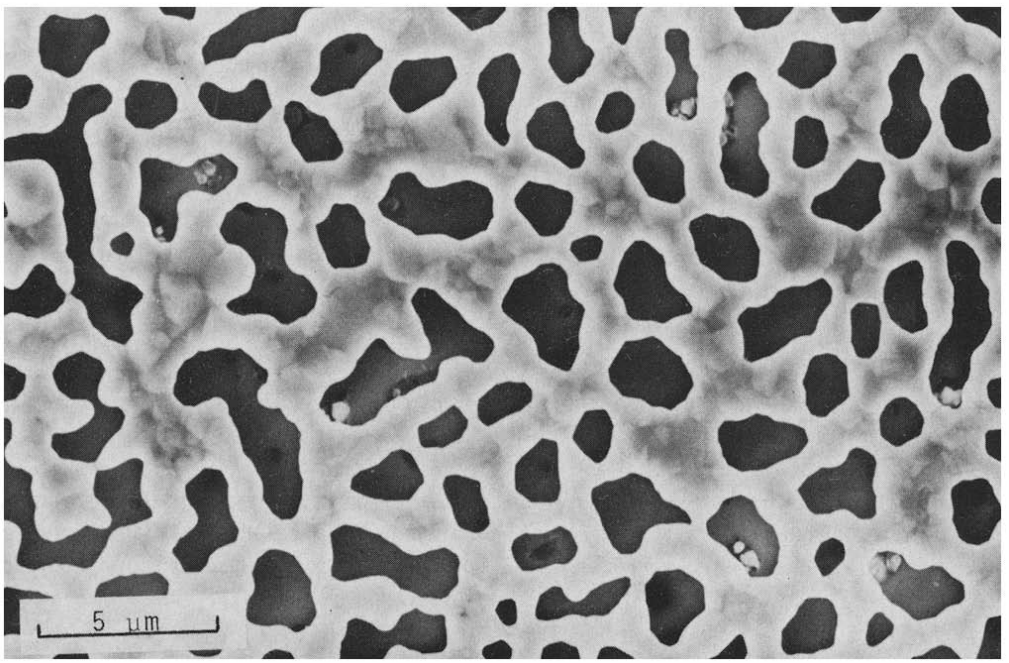

Fig. 1. Typical SEM picture of the sputtered platinum electrodes used in this study.

table 1. The $(ZrO_2)_{0.83}(YO_{1.5})_{0.17}$ (called ZY17) starting powder was prepared by the alkoxide method [10]. The Pt/ZY17/Pt system was placed in a Bi_2O_3 atmosphere as described elsewhere [11], after electrode resistance and response time measurements [12] on the Bi_2O_3 free system were performed. The electrode–electrolyte system, obtained in this way, is called ZYB1. This allows measurements of changes in R_{el} due to an atmosphere containing Bi_2O_3(g), which may adsorb on and react with the surface. The ZY21 and ZYB2 samples were prepared as described in [11]. All ceramic materials have a cubic (fluorite) structure and are monophasic.

The electrode–resistance measurements were performed on samples with a diameter of 10–13 mm and a thickness of 1–1.2 mm. The samples were polished with Al_2O_3 (0.05 µm). Platinum electrodes with a thickness of 170 (± 20) nm were sputtered onto the polished samples with a Balzers sputtering device. The thickness of the sputtered electrode was measured by a Balzers quartz thickness monitor (QSG 301). A mask was used during platinum sputtering at one side of the specimen. This mask separated the reference electrode from the counter electrode. The distance between these electrodes is 0.5 mm. The area of the reference electrode was kept small (about 7% of the total surface area). The opposite surface of the electrolyte which was completely covered with sputtered Pt was used as working electrode.

The sputtered samples were subjected to a temperature treatment of 2 h at 1220 K. This resulted in the porous electrode structure as shown in fig. 1. The samples were next treated in order to avoid changes in the results of electrical measurement during the measuring period. This consisted of a heat treatment at 1020 K for 48 h followed by an ac current treatment with 1 V (r.m.s.) at a frequency of 1 kHz during 5 min at 953 K (the highest measuring temperature). The morphology of the electrode is characterized by the length of the three phase line. This line is the contact line: gas–Pt electrode–electrolyte, and has a value of 9×10^5 m/m^2 for all samples.

The electrode resistance measurements were performed in a tubular furnace with a diameter of 40 mm at temperatures of 873 K and 953 K. The oxygen partial pressures in the range of 5×10^{-4}–1 atm O_2 were obtained by different O_2/N_2 mixtures. An Inacom mixing device was used with a gas supply rate of 40

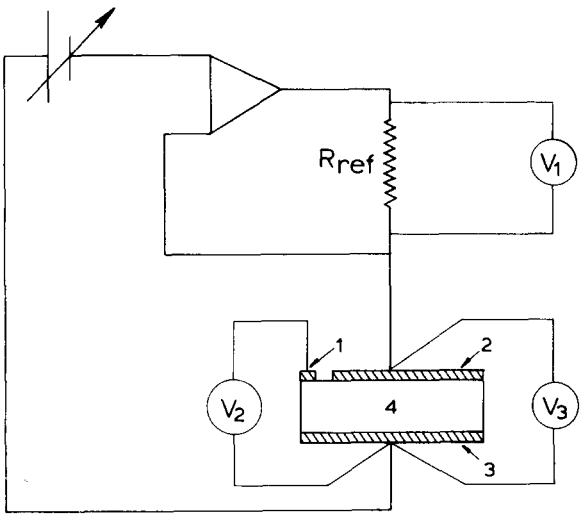

Fig. 2. Electrical circuit for the 3 point dc measurement; (1) reference electrode; (2) counter electrode; (3) working electrode; (4) electrolyte.

cm^3/min. The oxygen partial pressure of the gas mixtures was measured by an oxygen sensor based on stabilized zirconia.

The electrical circuit used for dc experiments is shown in fig. 2. A Wenking potentiostat was used in the voltage range of 1–10 mV. The different voltage drops were measured with HP 3465A multimeters. The current through the sample was calculated from the voltage drop across the reference resistor (V_1).

The ac complex impedance measurements were performed in the frequency range 10^6-10^{-3} Hz using a Solartron 1174 frequency response analyser with a sample voltage of 10 mV (r.m.s.). The circuit used in the ac experiments has been described elsewhere [13].

4. Results and discussion

4.1. dc polarization

The current–voltage relation shows an ohmic dependence in all cases at the small voltages used (1–10 mV). The current density through the samples is less then 6 A/m^2.

The potential drop between the reference and the working electrode (V_2 in fig. 2) equals the potential drop over the working electrode–electrolyte interface (deviation less than 10%). The voltage drop over the electrolyte is negligible for these materials, because low currents are used and the distance between reference and counter electrode is sufficiently large (here 0.5 mm). The contribution of the electrolyte polarization to V_2 cannot be neglected when higher currents are applied or when electrolyte material with higher conductivity is used. In that case the potential drop V_2 contains a contribution from the electrolyte, for which must be corrected. The electrolyte contribution to V_2 can be diminished by increasing the distance between reference and counter electrode.

The potential drop V_2 can be used to measure either the cathodic or the anodic process by reversing the current direction. In all cases the anodic resistance shows the same oxygen partial pressure dependence as the cathodic resistance and they are equal to each other within the accuracy of the measurements. These results suggest that the anodic and cathodic mass limiting current (I_{la} and I_{lc} in eq. (6) of sect. 2) are both much higher than the exchange current I_0 in the P_{O_2}, temperature and voltage region regarded. In the model we further use in this study, it is assumed that the charge transfer reaction is rate determining in the electrode process.

The sum of anodic and cathodic resistance is calculated as follows. The total potential drop over the electrolyte–electrode system is measured by V_3. The overall resistance is calculated from V_3 with the known current. The resistance across both electrodes is obtained by subtracting the electrolyte resistance, obtained from ac impedance measurements, from the overall resistance. The overall electrode resistances are given in fig. 3 for all samples as function of P_{O_2} after normalisation per unit area of the total electrolyte surface. A minimum in the R_{el}–P_{O_2} curves is found for all samples. The ZY17 sample showed a decrease in R_{el} after the treatment in Bi_2O_3 atmosphere (= sample ZYB1). At 953 K ZYB2 also shows a lower resistance than the Bi-free samples. The solid lines in fig. 3 represent an oxygen partial pressure dependency as indicated. The slopes of these lines have a deviation of at most 15% from the best fitted lines through these points.

The oxygen partial pressure dependences of R_{el} can be explained using eqs. (18) and (19) if the charge transfer process is the rate determining step in the electrode reaction. For samples modified with Bi_2O_3

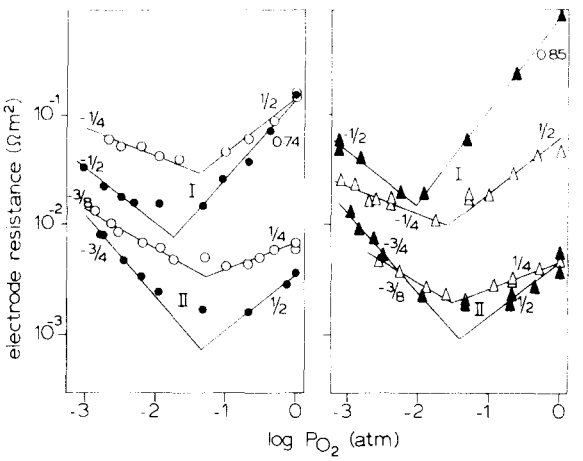

Fig. 3. Electrode resistance as a function of oxygen partial pressure at 873 K (I) and 953 K (II): (○) ZY17; (●) ZYB1; (△) ZY21; (▲) ZYB2. The solid lines represent a $P_{O_2}^n$ dependence. The value of n for each line is given in the figure.

(ZYB1 and ZYB2) the exponent n in the relation $R_{el} \sim P_{O_2}^n$ has a value which is twice that of Bi_2O_3-free samples (ZY17 and ZY21), except for relatively low temperature and high oxygen partial pressure (873 K and $P_{O_2} > 10^{-2}$ atm). This difference in P_{O_2} dependence (factor 2) is also found if the dissociative Langmuir-adsorption is compared with the associative one (cf. eqs. (3a) and (3b) in sect. 2). The values of the exponents in eqs. (18) and (19) for associative adsorption are twice those of dissociative adsorption. This suggests that oxygen adsorbs dissociatively on ZY17 and ZY21 and associatively on ZYB1 and ZYB2 samples. The oxygen molecule on the ZYB samples dissociates *after* adsorption. The reaction steps following the adsorption are then supposed to be exactly the same for pure and Bi-doped ZY and hence α_a and α_c have the same values for both types of material. It is not necessary in this case that the adsorption step is the rate limiting one.

The surface of a ZY17 sample placed in a Bi_2O_3 atmosphere showed an enrichment of Bi, which was detected by Auger electron spectroscopy. Auger analysis of a ZYB2 surface after a temperature treatment which is the same as applied during the electrode annealing treatment (2 h 1220 K and 48 h 1020 K) also shows enrichment of the surface with Bi. The surface composition amounts to about 15 mol% $BiO_{1.5}$ in both cases. The Bi percentage of the outermost surface layer may be larger but this is not detectable with Auger analysis. These results indicate that oxygen adsorbs associatively on Bi. The same phenomenon is mentioned by Sleight [14] who suggests that bismuth may serve as the adsorption site for molecular oxygen in oxidation catalysis on bismuth molybdates.

The case of dissociative adsorption on ZY17 and ZY21 is now regarded into some detail. The first mechanism we regard for the electrochemical reaction is a stepwise charge transfer reaction:

$$O_{r.s} + V_O^{\bullet\bullet} + e' \leftrightharpoons O_O^{\bullet} + V_{r.s} \,. \qquad (a)$$

$$O_O^{\bullet} + e' \leftrightharpoons O_O^{\times} \,. \qquad (b)$$

If the first step (a) of this reaction is rate determining the values of α_a and α_c are respectively 3/2 and 1/2 (eqs. (12) and (13) with $\gamma_a = 2$, $\gamma_c = 0$, $r = 1$ and $\nu = 2$). This results in $R_{el} \sim P_{O_2}^{1/8}$ for high P_{O_2} ($\theta \approx 1$) and $R_{el} \sim P_{O_2}^{-3/8}$ for low P_{O_2} ($1 - \theta \approx 1$) using eqs. (18a) and (19a) respectively. The behaviour of $R_{el} \sim P_{O_2}^{-3/8}$ was experimentally found at 953 K and $P_{O_2} < 3 \times 10^{-2}$ atm (see fig. 3).

The charge transfer reaction may also proceed by a two-electron mechanism:

$$O_{r.s} + 2e' + V_O^{\bullet\bullet} \leftrightharpoons O_O^{\times} + V_{r.s} \,.$$

The anodic and cathodic transfer coefficients are equal ($\alpha_a = \alpha_c = 1$) if this overall charge-transfer reaction is rate determining. This results in $R_{el} \sim P_{O_2}^{1/4}$ for high P_{O_2} and $R_{el} \sim P_{O_2}^{-1/4}$ for low P_{O_2}. This behaviour was experimentally found at high P_{O_2} ($>3 \times 10^{-2}$ atm) and 953 K as well as for low P_{O_2} ($<10^{-2}$ atm) and lower temperatures (873 K).

Berry [15] found that platinum oxide was formed at an oxygen partial pressure of 1 atm and a relatively low temperature of 850 K. The results of Berry suggest that at 873 K and relatively high P_{O_2} a chemisorbed oxygen layer can be formed on the platinum electrode surface. The electrode reaction can now be described by the following steps:

$$O_{r.s} + 2e' \leftrightharpoons O_{r.s}^{2-}\,(Pt) \,, \qquad (c)$$

$$O_{r.s}^{2-}\,(Pt) + V_O^{\bullet\bullet} \leftrightharpoons O_O^{\times} + V_{r.s} \,. \qquad (d)$$

If the last step (d), which takes place on the three phase line, is rate determining the values of α_a and α_c are 0 and 2 respectively ($\gamma_a = 0$, $\gamma_c = 4$, $r = 0$ and $\nu = 2$ in eqs. (12) and (13)). The electrode resistance at

high P_{O_2} is then proportional to $P_{O_2}^{1/2}$ (eq. (18a)), which experimentally was found for Bi_2O_3-free samples at 873 K and $P_{O_2} > 4 \times 10^{-2}$ atm (see fig. 3). The same mechanism should give $R_{el} \sim P_{O_2}^{1}$ for bismuth doped samples where associative adsorption is expected. The slopes in the R_{el}–P_{O_2} figure tend to reach this value for ZYB specimen at $P_{O_2} > 10^{-2}$ atm and $T = 873$ K. Here probably associative and dissociative mechanisms operate in parallel resulting in an intermediate exponent.

The electrode reaction mechanisms suggested here cannot easily be compared with literature. Verkerk et al. [1] concluded from theoretical calculations that probably the electrode process for sputtered platinum electrodes on ZY17 was determined by mass transport over the anode at high P_{O_2} and mass transport over the cathode at low P_{O_2}. This contradiction with our results may be due to the investigated temperature region. The lower temperatures used in this investigation (873–953 K) instead of the temperatures around 970 K from which Verkerk et al. [1] have mainly drawn their conclusions) suggests a charge-transfer mechanism as was also found by Mizusaki et al. [16] at 873 K. The stronger P_{O_2} dependence of R_{el} observed by Verkerk [1] may also be due to some bismuth contamination on the electrode–electrolyte surface of which the authors were not aware. In future electrode resistance measurements will be performed in a temperature region covering the complete range (873–1000 K).

4.2. ac impedance measurements

The complex impedance diagrams of some samples at a temperature of 953 K and an oxygen partial pressure of 0.012 atm are given in fig. 4. Both, the shape of these diagrams and the impedance values change with oxygen partial pressure and are therefore associated with the electrode behaviour of these samples. This was also indicated by a four probe dc measurement on ZY17, where the electrolyte resistance equals the resistance calculated from the high frequency intercept at the left hand side in fig. 4. The results of the electrolyte impedance measurements, which show a bulk and grain boundary contribution, are published elsewhere [12]. The electrode data are analysed by means of a circuit which incorporates a Constant Phase Angle (CPA) element. This element can be written as an impedance [17,18]:

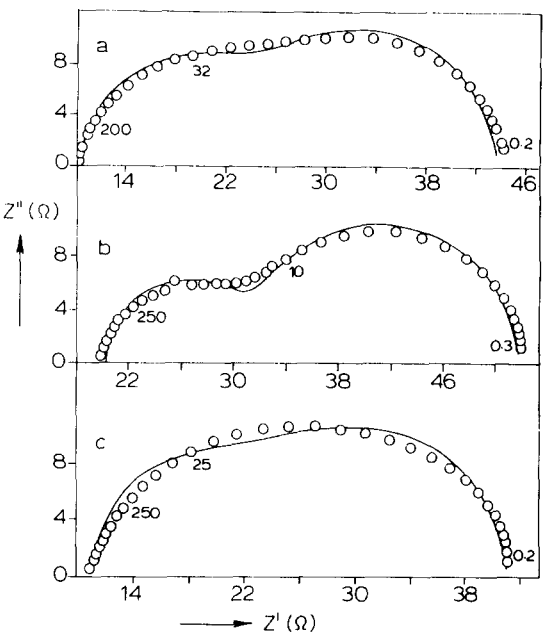

Fig. 4. Complex impedance diagrams for the electrode behaviour at $T = 953$ K and $P_{O_2} = 1.2 \times 10^{-2}$ atm; (a) ZY17, (b) ZY21, (c) ZYB2. The frequency is given in Hz; (o) experimental data. The solid line is the best fitted result of the electrical circuit, given in fig. 6.

$$Z(\mathrm{CPA}) = A_0^{-1}(j\omega)^{-\beta} \quad \text{with} \quad 0 \leqslant \beta \leqslant 1 \,.$$

The components of the modulus $Z = Z' - jZ''$ are:

$$Z' = A_0^{-1}\,\omega^{-\beta}\cos[(\pi/2)\beta] \,,$$

$$Z'' = A_0^{-1}\,\omega^{-\beta}\sin[-(\pi/2)\beta] \,,$$

where ω is the angular frequency. The CPA impedance represents a resistor if $\beta = 0$ ($A_0 = R^{-1}$), a capacitance if $\beta = 1$ ($A_0 = C$) and a Warburg impedance if $\beta = 0.5$. At intermediate values of β no clear physical meaning is known for the CPA element.

The experimental data of ZY21 and ZYB2, as given in figs. 4b and 4c respectively, could be described by a series combination of a resistance and two circuits; each circuit consists of a CPA element and a resistance in parallel (see fig. 5). This overall circuit was analysed by a non-linear least square fitting program [18]. The relative deviation of the measured data from the calculated data by the program was within 2%. The values of β in the CPA's in ZY21 are 0.87 and 0.93 for the high and low frequency parts respectively, while for ZYB2

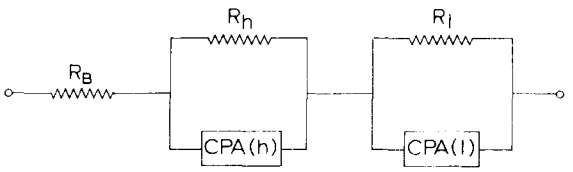

Fig. 5. Electrical circuit, which gives the best results for the experimental data of fig. 4. CPA = Constant Phase Angle, h and l indicate high and low frequency part respectively; R_B: overall electrolyte resistance.

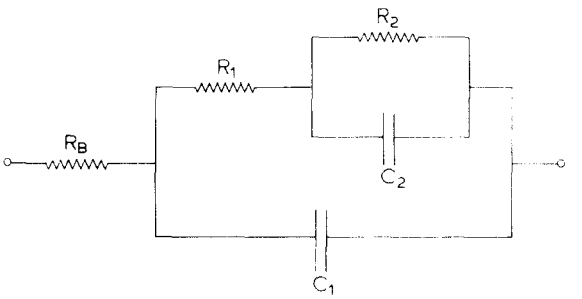

Fig. 6. Electrical circuit represented by the solid lines in fig. 4.

these values are 0.8 and 1. These CPA's most resemble a capacitance ($\beta = 1$). The parallel R–CPA circuits can therefore be regarded as R–C circuits with $C = (AR^{1/\beta})/R$ and a depression angle $\alpha = (1-\beta)\pi/2$ below the Z' axis of the semicircle representing the R–C circuits. The depression angle (18° for $\beta = 0.8$ or smaller for higher β values) may be due to a discrete number of series and parallel reaction steps in the charge transfer process [19]. This point will not be further discussed because there are also a number of trivial reasons which can give rise to the depression angles observed here (in most cases smaller than 12°); e.g., electrolyte surface roughness and an inhomogeneous electrode–electrolyte interface.

The data calculated by the fitting program did not show any classical Warburg impedance behaviour ($\beta = 0.5$). No frequency dispersion was observed at frequencies lower than induced in fig. 4 (down to 10^{-3} Hz). A Warburg impedance is physically connected with a diffusion process on the electrode or electrolyte. The ac results support the assumption that diffusion of oxygen from adsorption site to reaction site or reverse is not rate determining under the conditions regarded here being a relatively low temperature and relatively high oxygen partial pressure ($>10^{-2}$ atm). The presence of a R-type Warburg behaviour [2,20] cannot be excluded, however. The depression at high frequencies observed in fig. 4c may be due to the onset of a diffusion limiting process.

The ac frequency dispersion measurements on ZY17, ZY21 and ZYB2 at 873 K and 953 K and 10^{-2} atm $\leqslant P_{O_2} \leqslant 1$ atm show the same kind of impedance diagrams as shown in fig. 4. These results are further analysed by the electrical circuit given in fig. 6. The total electrolyte resistance is given by R_b. The electrode impedance is represented here by simple RC circuits (R_1, R_2, C_1, C_2). The circuit in fig. 6 is represented in a complex impedance diagram by two (partly) overlapping semicircles with a depression angle of 0°. The calculated results by the fitting program [18] are given by the drawn lines in fig. 4. Badwal et al. [21,22] also found similar types of diagrams for Pt or Pd sputtered electrodes on yttria-stabilized zirconia in the temperature region of 873–1273 K. The high frequency part of the electrode polarization, which is represented by R_1 and C_1 in fig. 6, is relatively constant in the P_{O_2} and temperature region regarded. The (double layer) capacity, C_1, has a value of 1–3.5 F/m^2. These values are also found in literature for the same type of systems [16,23].

The low frequency part (R_2 and C_2 in fig. 6) shows a strong variation in C_2 values (4–40 F/m^2) depending on P_{O_2} and T. A quantitative correlation cannot be made due to a large scatter in the results. There is, however, a tendency of a decrease in C_2 as well as in C_1 when the oxygen partial pressure increases from 10^{-2} atom to 1 atm (see table 2). Verkerk et al. [2] found a decrease in low frequency capacity for sputtered Pt electrodes on ZY17 when P_{O_2} decreases from 5×10^{-2} atm to 10^{-4} atm. This result suggests that a maximum is present in the C_2–P_{O_2} relation. The decrease of C_2 and C_1, we observe may be due to a de-

Table 2
Capacitance values of the elements in fig. 6 at 953 K.

P_{O_2} (atm)	ZY17		ZYB2	
	C_1 (F/m^2)	C_2 (F/m^2)	C_1 (F/m^2)	C_2 (F/m^2)
0.012	3.8	38	3.5	20
0.04833	3.2	43	2.3	10
1	2.5	13	1.7	7.4

crease in effective reaction surface for the electrode reaction.

The electrode behaviour of Bi_2O_3 doped yttria-stabilized zirconia differs from that of stabilized Bi_2O_3 systems. The electrode resistance of Er_2O_3 stabilized Bi_2O_3 was found to be considerably lower than that of ZY17, while no minimum in the R_{el}–P_{O_2} curve was found [1]. The complex impedance measurements on Bi–Er clearly showed a classical Warburg behaviour at $P_{O_2} > 10^{-1}$ atm which is associated with surface diffusion (of electron holes) as limiting step in the electrode process [2]. This difference between ZYB and Bi_2O_3–Er_2O_3 systems indicate that the structure of the bismuth-rich layer is important for the electrode behaviour of Bi-doped samples.

5. Conclusions

The anodic and cathodic resistance of both bismuth-free and Bi_2O_3-doped yttria-stabilized zirconia show the same oxygen partial pressure (P_{O_2}) dependence at *low* over-voltages and current densities. This result indicates a model where charge transfer is the rate determining step for the electrode reaction in the temperature, P_{O_2} and voltage region regarded.

A ZY17 specimen with a Bi-rich surface shows a somewhat lower R_{el} than pure ZY17.

The relation between R_{el} and P_{O_2} can be represented by $R_{el} \sim P_{O_2}^n$. For Bi_2O_3 doped materials the value of n is twice that for Bi-free materials. This P_{O_2} dependence of R_{el} can be explained in a consistent way if it is assumed that oxygen adsorbs dissociatively on the bismuth free and associatively on the bismuth doped samples.

The ac impedance behaviour of the electrodes can be analysed by simple R–C circuits. No classical Warburg impedance was observed in P_{O_2} range of 10^{-2}–1 atm. The electrode capacity values indicate that the effective reaction surface for the electrode reaction decreases with increasing P_{O_2} at these relatively high oxygen partial pressures used ($P_{O_2} > 10^{-2}$ atm).

Acknowledgement

We would like to thank Dr. K.J. de Vries, Dr. D.W.M. van den Ham and Drs. M.P. van Dijk for their stimulating discussions.

References

[1] M.J. Verkerk, M.W.J. Hammink and A.J. Burggraaf, J. Electrochem. Soc. 130 (1983) 70.
[2] M.J. Verkerk and A.J. Burggraaf, J. Electrochem. Soc. 130 (1983) 78.
[3] L.J. Olmer and H.S. Isaacs, J. Electrochem. Soc. 129 (1982) 345.
[4] J. Fouletier, H. Seinera and M. Kleitz, J. Appl. Electrochem. 4 (1974) 305.
[5] J.E. Bauerle, J. Phys. Chem. Solids 30 (1969) 2657.
[6] S. Pizzini, in: Fast ion transport in solids, ed. W. van Gool (North-Holland, Amsterdam, 1973) p. 461.
[7] D.Y. Wang and A.S. Nowick, J. Electrochem. Soc. 126 (1979) 1155.
[8] H. Okamoto, G. Kawamura and T. Kudo, Electrochim. Acta 28 (1983) 379.
[9] J.O.M. Bockris and A.K.N. Reddy, in: Modern electrochemistry, Vol. 2 (Plenum Press, New York, 1973) ch. 9.
[10] M.A.C.G. van de Graaf, J.H.H. ter Maat and A.J. Burggraaf, in: Ceramic powders, ed. P. Vincenzini (Elsevier, Amsterdam, 1983) p. 783.
[11] A.J.A. Winnubst and A.J. Burggraaf, Mat. Res. Bull. 19 (1984) 613.
[12] A.J.A. Winnubst, A.H.A. Scharenborg and A.J. Burggraaf, J. Appl. Electrochem., to be published.
[13] M.J. Verkerk, B.J. Middelhuis and A.J. Burggraaf, Solid State Ionics 6 (1982) 159.
[14] A.W. Sleight, in: Advanced materials in catalysis, eds. J.J. Burton and L. Garten (Academic Press, New York, 1977) p. 181.
[15] R.J. Berry, Surface Sci. 76 (1978) 415.
[16] J. Mizusaki, K. Amano, S. Yamauchi and J. Fueki, in: Chemical sensors, ed. T. Seijama (Elsevier, Amsterdam, 1983) p. 277.
[17] P.H. Bottelberghs and G.H.J. Broers, J. Electroanal. Chem. 67 (1976) 155.
[18] B.A. Boukamp, Solid State Ionics 11 (1984) 339.
[19] H.J. de Bruin and A.D. Franklin, J. Electroanal. Chem. 118 (1981) 405.
[20] H.T. Cahen, Ph.D. Thesis, State University Utrecht (1980).
[21] S.P.S. Badwal, J. Electroanal. Chem. 146 (1983) 425.
[22] S.P.S. Badwal and H.J. de Bruin, J. Electrochem. Soc. 129 (1982) 1921.
[23] D.Y. Wang and A.S. Nowick, J. Electrochem. Soc. 126 (1979) 1166.